Wear 309 (2014) 247–255

Contents lists available at ScienceDirect

Wear

journal homepage: www.elsevier.com/locate/wear

Effect of reinforcement type, size, and volume fraction on the tribological behavior of Fe matrix composites at high sliding speed conditions

T. Ram Prabhu [a], V.K. Varma [a], Srikanth Vedantam [b,*]

[a] Centre for Military Airworthiness and Certification, Marathalli Colony Post, Bangalore, India
[b] Department of Engineering Design, Indian Institute of Technology Madras, Chennai, India

ARTICLE INFO

Article history:
Received 26 April 2013
Received in revised form
30 September 2013
Accepted 4 October 2013
Available online 11 November 2013

Keywords:
A. Sliding wear
B. Metal-matrix composite
C. Brakes/clutches
D. Wear testing

ABSTRACT

In this paper we studied the tribological behavior of iron matrix composites at high sliding speeds (25–35 m/s) typical of aircraft braking conditions. We developed two types of Fe matrix composites with different elastic modulus reinforcements: silica (71 GPa) and mullite (143 GPa) particulates using powder metallurgy. Two different size ranges: large (150–250 μm) and small sizes (1–10 μm) and a range of volume fractions of the particulates were also considered. The dry sliding wear and braking performance of the composites were investigated using a sub-scale disc braking dynamometer. The wear tests of the composites show that large size and high volume fraction of reinforcement particles provides better wear resistance and braking performance at high sliding speed conditions (25 m/s–35 m/s) for both Fe/silica composites and Fe/mullite composites. Significantly, Fe/mullite composites at lower volume fractions showed greater wear resistance than the Fe/silica composites due to the higher elastic modulus of the mullite particles. A wear track examination of composites showed that different wear mechanisms were operative at the different speeds. Our results indicate that composites with a high volume fraction of large sized reinforcement particles of high elastic modulus are to be preferred for braking performance and low wear loss at high sliding speed applications.

1. Introduction

Metal matrix composites (MMCs) are promising candidates for high temperature wear applications such as in jet engines, gas turbine seals and bearings, brakes and clutches. The compatibility between the various metal matrix and ceramic reinforcement materials makes it possible to obtain diverse thermal, mechanical and tribological properties of these MMCs. The reinforcements in MMCs may be either long, continuous, multi-strand fibers or discontinuous particulates. Reinforcements in fiber form are generally not used in braking material applications due to the possibility of fiber breakage, microstructural non-uniformities, interface failure and anisotropic properties [1–3]. Particulate metal matrix composites (pMMC) are therefore mostly preferred for brake friction materials applications.

Currently, most of the tribological studies of pMMCs are based on either aluminum or copper matrix based particulate composites due to their attractive properties such as high thermal conductivity, specific heat capacity, corrosion resistance, low density and compatibility with SiC and Alumina as reinforcements [3–14]. However, these studies have been until now mostly conducted using typical pin and disc wear tests at low loads (<100 N) and sliding speeds (<4 m/s). At higher sliding speeds and loads, the temperature rise at the sliding interface may be so high that an Al or Cu matrix may soften, and in extreme cases melt, due to their low melting point and low strength at high temperatures. Thus, Al or Cu as matrix materials may not be suitable for such high energy braking applications such as in race cars, high speed trains, trucks and aircraft brakes.

Alternatively, for such high energy applications, iron has been considered as a matrix material. The high melting point, high work hardening rate, better strength, heat resistance properties and, most importantly, the low cost and abundance make it a desirable choice [15]. The dry sliding wear behavior of Fe/SiC particulate composites has been studied at low loads (5–25 N) and low sliding speeds (2.5–6 m/s) [16,17]. It was found that Fe/SiC composites have excellent abrasive wear resistance and can be used in dry sliding applications under these conditions. Fe/SiC has also recently been found to perform well at high load and speed conditions [18].

Currently, relatively high cost carbides and nitrides such as SiC, B_4C, TiC and Si_3N_4 are the most commonly used reinforcements in

* Corresponding author. Tel.: +91 44 22574739; fax: +91 44 22574732.
E-mail address: srikanth@iitm.ac.in (S. Vedantam).

0043-1648/$ - see front matter © 2013 Elsevier B.V. All rights reserved.
http://dx.doi.org/10.1016/j.wear.2013.10.001

metal matrix composites due to their high hardness and wear resistance properties [19–21]. However, the possibility of extensive interfacial reactions and oxidation of carbides and nitrides at elevated temperatures are still concerns which need to be addressed before use in high energy braking friction applications. Alternatively, there have been a few attempts to replace these reinforcements with relatively lower cost oxide reinforcements (silica or mullite) in Al matrix composites [22–24]. In particular, Hemanth [24] showed that the addition of 9 wt% silica in A356 Al alloy improved wear resistance and mechanical properties of the composites. An added advantage of using oxide reinforcements is that their presence may act as an effective barrier against interfacial reactions [25].

There have been few wear studies of pMMCs at high sliding speed conditions appropriate to aircraft braking applications. Some recent studies have focused on the wear behavior of pMMCs at relatively high braking speed conditions (up to 12 m/s), but were specific to automobile applications [26–29]. To the best of our knowledge, the combination of Fe matrix with oxide particulate reinforcements (silica or mullite) has not yet been developed and studied for high speed tribological applications. Considering this gap in previous studies, we have undertaken to prepare and systematically study the tribological behavior of Fe matrix composites for high sliding speed conditions (25–35 m/s).

We organize this paper as follows. In the following section, we describe the preparation of the Fe matrix composites (Fe/SiO_2 and Fe/mullite) and the test procedures. In Section 3, we present the results of wear loss and braking performance of Fe matrix composites tested for braking speeds of 25–35 m/s. Next, the effect of size and volume fraction of the particulates (silica and mullite) on the wear and frictional properties of Fe matrix composites was critically analyzed. The wear tracks of the composites: Fe/30%silica (large and small size particles), Fe/20%mullite (large particles) and Fe/15%mullite (small particles) were examined under a stereo microscope. Based on the observed wear features, the potential wear mechanisms are discussed.

2. Experimental details

2.1. Materials

The composites were prepared by powder metallurgy (PM) process using commercial grade powders of Fe, silica, mullite, barium sulphate ($BaSO_4$) and graphite of more than 97% purity. The size of the particles in the constituent powders are given in Table 1. The composition and identification of Fe/silica composites and Fe/mullite composites are given in Tables 2 and 3 respectively. The as-received form of silica or mullite powders consisted of particles in a size range of 150 – 250 μm. These large size particulates of silica or mullite were milled in vibratory ball mill to reduce the sizes to the submicron range. A ball to powder ratio of 6:1 and milling time of 12 h were used to prepare the small particles size silica and mullite powders. The composite powder mixes were obtained by following the mixing sequence shown in Fig. 1. The powder mix was cold

Table 2
Details of the chemical composition in vol % and designations of the Fe/silica composites.

Group	Designation	Silica (%)	$BaSO_4$ (%)	Graphite (%)	Iron
LO	LO-A	10	7	18–19	Balance
	LO-B	20	9	18–19	Balance
	LO-C	30	11	18–19	Balance
SO	SO-A	10	7	18–19	Balance
	SO-B	20	9	18–19	Balance
	SO-C	30	11	18–19	Balance

Table 3
Details of the chemical composition in vol % and designations of the Fe/mullite composites.

Group	Designation	Mullite (%)	$BaSO_4$ (%)	Graphite (%)	Iron
LM	LM-A	10	7	18–19	Balance
	LM-B	15	9	18–19	Balance
	LM-C	20	11	18–19	Balance
SM	SM-A	10	7	18–19	Balance
	SM-B	15	9	18–19	Balance

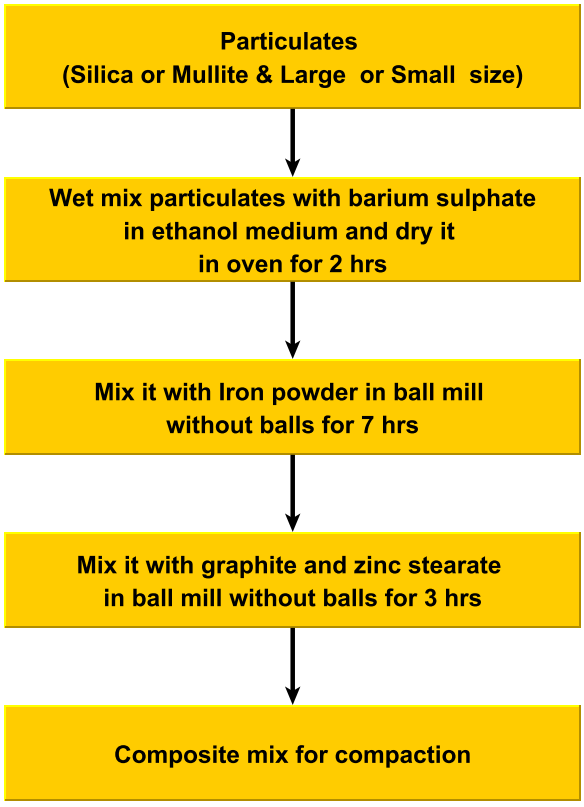

Fig. 1. Mixing procedure of the composite mixes.

Table 1
Sizes of the particles in the powders used.

Type of powder	Silica	Mullite	$BaSO_4$	Graphite	Iron
Particulate size range (μm)	150–250[a], 0.7–7[b]	150–250[c], 2–10[d]	53–63	60–90	125–150

[a] Composites LO.
[b] SO.
[c] LM.
[d] SM.

compacted for 30 s at a pressure of 450 MPa in a single uniaxial die compaction press. Before each compaction operation, a single coat of zinc stearate was applied on the die and the punch to facilitate easy ejection of the green compact. It is noted that any attempt at exceeding the maximum limit of reinforcement of silica or mullite in the Fe matrix resulted in cracking during green compact ejection. Ni plated plain carbon steel (Fe-0.15–0.25% C) sheets of 1.2 mm thickness and maximum hardness of 162 BHN were used as backing plates for the composite brakepads. Pressure sintering was used to bond the steel strip and the green compact. The sintering was carried out at a pressure of 25 MPa and temperature of 1020 °C for 3 h in a dry hydrogen protective atmosphere in a Bell furnace. The sintered composite brakepads were again pressed at a pressure of 300 MPa for 30 s to improve their density, dimensional accuracy and to eliminate the residual stresses developed during sintering.

2.2. Test procedures

2.2.1. Physical and mechanical characterization

The density of Fe/silica and Fe/mullite composites was determined using Archimedes' principle. The samples were first weighed in air and then in water using a Mettler Toledo electronic balance with 0.5 g accuracy. The void fraction of sintered composites is taken to be

$$v_f = \frac{\rho_t - \rho_m}{\rho_t}, \quad (1)$$

where v_f is the void fraction, ρ_t the theoretical density calculated using the rule of mixtures and ρ_m is the density measured using Archimedes' principle.

The hardness was measured on a Brinell scale with a steel ball indenter of 1 mm diameter and a load of 10 Kg using a Wolpert universal hardness testing machine.

2.2.2. Sliding wear test

Fe/silica and Fe/mullite composites were tested in a sub scale pad-on-disk dynamometer braking test system (schematically shown in Fig. 2) to study the wear and friction behavior. The pad-on-disk wear testing unit represents a typical flat on flat sliding condition. A gray cast iron disc (Grade: AMTY 273-68, C: 3.3.6%, Si: 1.6–2.3%) was used as the rotor in our study. The diameter and hardness of the rotor were 500 mm and 225 BHN respectively. The swept area and radius of the wear path were 3352.4 mm^2 and 51.5 mm (measured between the inner and outer edges of the pad) respectively. The composite brake pads were mounted on the braking piston. The mass moment of inertia of the flywheel was 49 Nms^2 and the applied constant brake force was 1323 N. The rotor was set to the desired braking speeds (25 m/s, 30 m/s and 35 m/s) by accelerating the flywheel using a 110 kW DC electric motor. The application of brake force on the brake pads established the frictional contact between the brake pads and rotor, and stopped the rotor. The braking parameters such as stopping distance, stopping time, mean torque and coefficient of friction (CoF) were recorded by a data acquisition system. Before conducting the tests on a new composition brake pad, a bedding-in operation was carried out to burnish the disc and brakepads. The burnishing procedure consisted of runs and braking stops from a speed of 5 m/s to the actual testing speed (with steps of 5 m/s at the actual testing brake pressure). After each of such runs, sufficient time was given for a brake pad and disc to cool to room temperature. The brake discs were thoroughly cleaned with proprietary brake cleaning agents to eliminate grease, surface residue and any debris between tests. Next, braking parameter data of the coefficient of friction and stopping distance for first 5 brake stops of actual testing speed were checked for consistency. If data was consistent and the visual showed the pad surfaces to be even, then the actual test is carried out. For each pad, 20 braking stops were performed to collect the braking parameters data. The pads were cleaned in acetone before and after each test and weighed in an Osaka Digital electronic balance with accuracy of 0.01 g to determine wear loss (by mass).

2.2.3. Microscopic examination

The microstructure of the Fe/silica (LO-C, SO-C) and Fe/mullite composites (LM-C, SM-B) was examined in a Nikon Epiphot optical microscope to analyze the distribution of the particulates and phases present. The bond quality between the composite and the back plate were also examined.

A SEIWA stereo microscope was used to examine the wear tracks of the composites. The sizes of the large size silica and mullite particulates were determined by sieve analysis. The BS-410 standard was used to convert the sieve mesh number to particulate size. In the case of small size silica and mullite particulates, the sieve analysis could not be employed due to the sub micron sizes and the size ranges were measured from scanning electron microscopy (SEM) images using an image analysis software (ImageJ). Spot energy dispersive X-ray analyses (EDAX) were also performed on the particulates of sintered composites to detect and identify the presence of any interfacial reaction products.

3. Results and discussion

3.1. Morphology and size of the silica and mullite particulates

The sieve analysis of the as-received form of silica and mullite particulates showed particles of sizes ranging from 150 to 250 μm (sieve mesh number: −60/+100). The SEM images analysis of the ball milled particulates of silica and mullite indicated that the

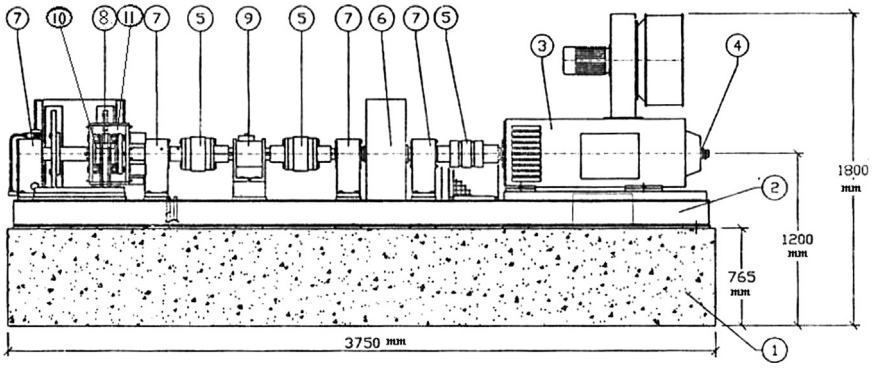

Fig. 2. A schematic of the pad-on-disk dynamometer braking test system. (1) Concrete base. (2) Structure. (3) D.C motor. (4) Encoder. (5) Torsional rigid coupling. (6) Flywheel. (7) Bearing housing. (8) Gray cast iron rotor. (9) In-line rotating torque transducer. (10) Brakepads. (11) Brake caliper assembly.

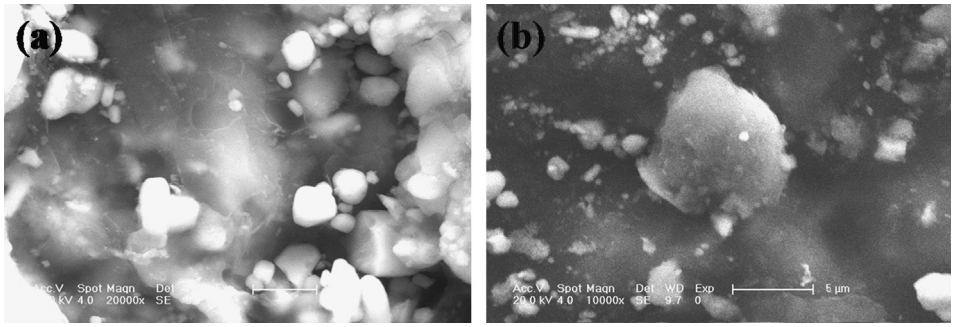

Fig. 3. SEM images of (a) small size silica particulates and (b) small size mullite particulates showing the size ranges of 0.7–7 μm and 2–10 μm, respectively.

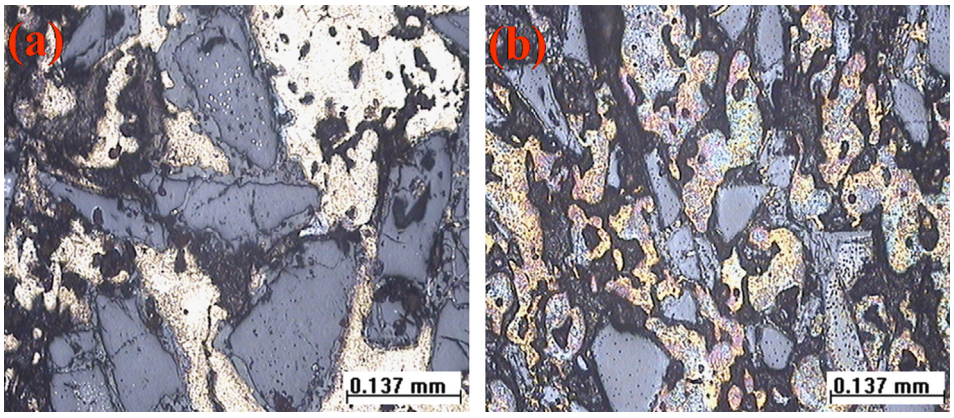

Fig. 4. Microstructure of Fe/Silica composites. (a) LO-C, (b) SO-C. A uniform distribution of silica and graphite is observed in the pearlitic iron matrix.

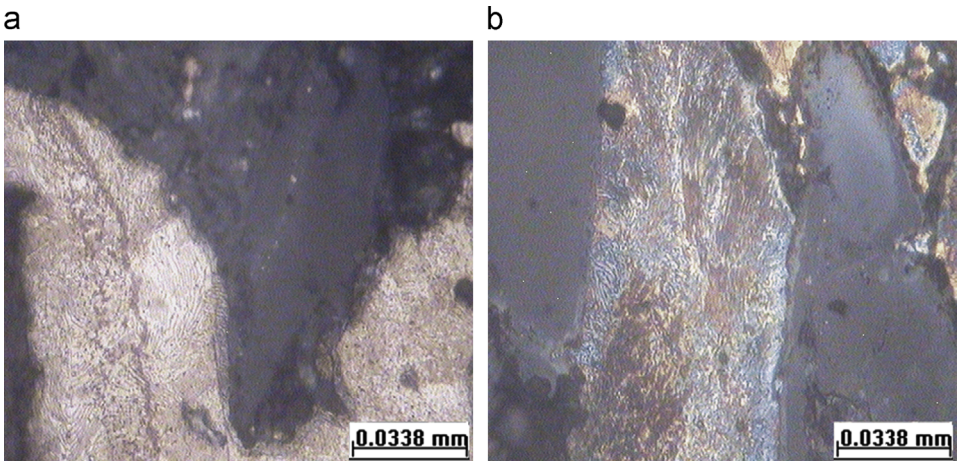

Fig. 5. Matrix microstructure of Fe/Silica composites. (a) LO-C, (b) SO-C. Clear pearlite lamellar structure is observed in the matrix.

particles were of sizes ranging from 0.7 to 7 μm and 2 to 10 μm respectively. The morphology of both the particulates was approximately spherical, as seen in Fig. 3. The EDAX spectra of the particulates in the composites (not shown) confirmed the presence of only particulate elements and the absence of any undesirable interfacial reaction products at the matrix/particulate interface.

3.2. *Microstructural studies*

A microstructural analysis of the Fe/silica composites (Fig. 4 (a) and (b)) and the Fe/mullite composites (not shown) shows that the particulates are uniformly distributed throughout matrix. A higher magnification image of the composites (Fig. 5 for Fe/silica composites) shows a distinct pearlite phase constituting a major portion of the matrix. The diffusion of carbon from the graphite into iron during sintering is responsible for the formation of the pearlite phase in the matrix.

The cross sectional view of brake pads of LO-C, SO-C, LM-C and SM-B composites shown in Fig. 6(a)–(d) respectively, presents three distinct layers: (i) the steel back plate showing ferrite and pearlite phases, (ii) an intermediate Ni layer of 70–100 μm thickness, and (iii) the composite layer. The bond between the back plate and the composite was achieved by the intermediate Ni layer. The purpose of the back plate is to protect the composite from sudden, catastrophic failure caused by the complex dynamic

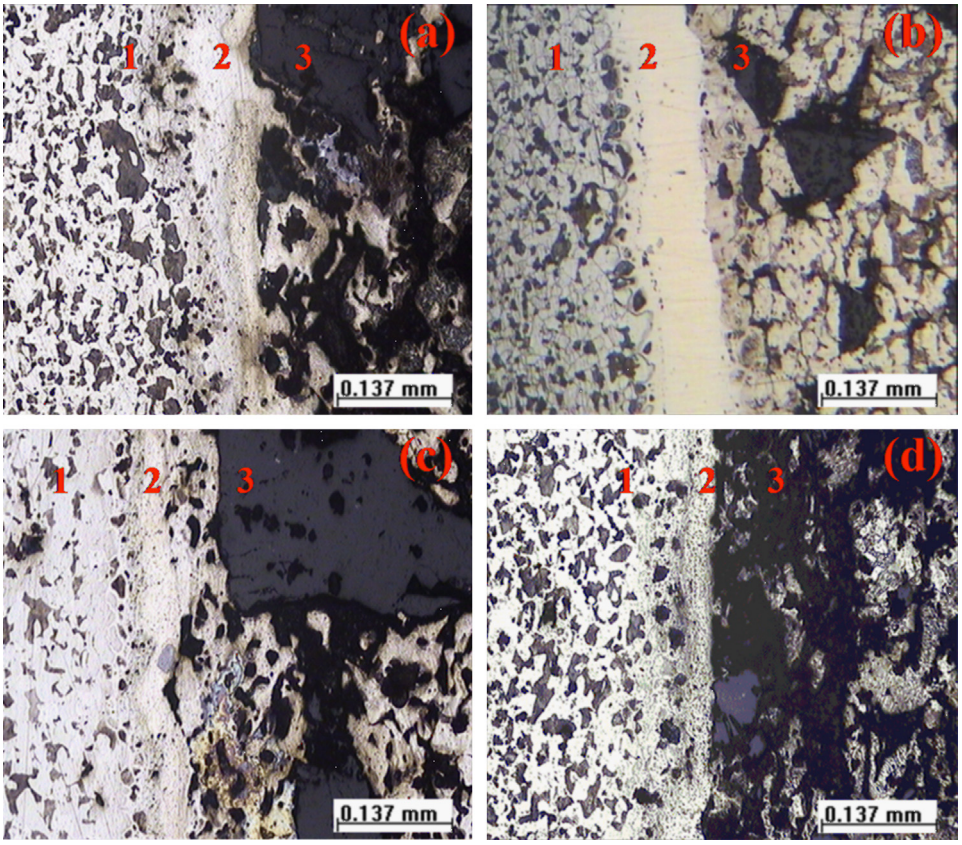

Fig. 6. Cross sectional microstructure of Fe/silica composites ((a) LO-C and (b) SO-C) and Fe/mullite composites ((c) LM-C and (d) SM-B). (1) Back plate showing ferrite and pearlite phases. (2) Ni plated layer. (3) Composite layer.

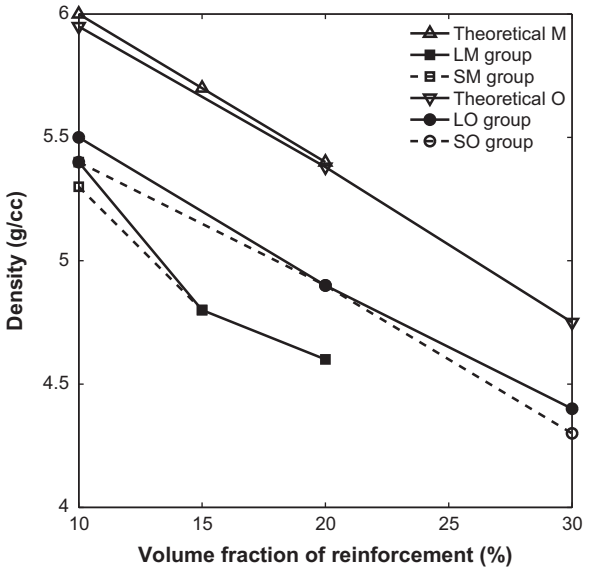

Fig. 7. Density of the silica and mullite reinforced composites as a function of the volume fraction of the reinforcement.

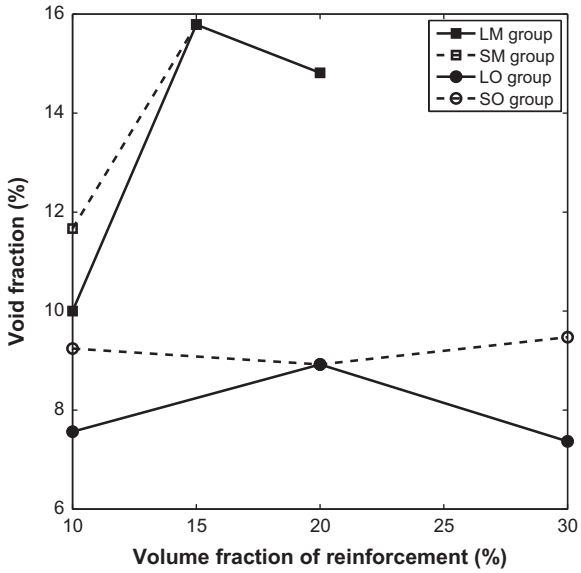

Fig. 8. Void fraction of the silica and mullite reinforced composites as a function of the volume fraction of the reinforcement.

loading during service. In addition, it also enhances the dimensional stability of the brake pad.

3.3. Density and void fraction

The density of two composites as a function of the volume fraction of the reinforcement is shown in Fig. 7. The density of the composites reduces with increasing volume fraction of the lower density particulates (silica $\rho = 2.2$ g/cc and mullite $\rho = 3.1$ g/cc). The effect of size of the particulates was insignificant in the density of the composites. A constant difference is observed between the experimental values of the density of the Fe/silica composite and the theoretical density calculated from the volume fractions of the constituents. However, the measured density of the Fe/mullite composite differs increasingly from the theoretical density with increasing volume fraction of mullite. This is due to

an increase in the void fraction (as seen in Fig. 8) of the Fe/mullite composite with volume fraction of the reinforcement. On the other hand, the void fraction is constant as a function of the volume fraction in Fe/silica composites. The increase in void fraction with volume fraction of mullite could be due to increased agglomeration or cluster formation, as reported in the case of other Fe based MMCs [20].

We note that the maximum volume fraction of mullite in the Fe matrix (20% in the case of LM group and 15% in the case of SM group) is limited due to relatively poor compatibility between the Fe and the mullite as evident from the greater void fraction. As a result of the high porosity it was not possible to prepare Fe/mullite MMCs with volume fraction of mullite greater than 20%.

3.4. Hardness

The hardness of the silica and mullite reinforced composites as a function of the volume fraction of the reinforcement is shown in Fig. 9. The increase in hardness with increasing volume fraction is due to the strengthening effect of the hard silica particulates. The presence of the second phase particulates enhances the strength of the composites, perhaps due to the generation of a high dislocation density during differential thermal contraction of the matrix and particulates and plastic deformation in the repressing operation. Other mechanisms such as the overall geometric constraint during deformation, dislocation–dislocation and dislocation–particulates interaction, and shearing of the particulate by dislocations during deformation may also result in the higher strength [25]. A similar observation of increasing hardness with volume fraction of the reinforcement was reported in Fe matrix composites by [16].

It may also observed from Fig. 9 that the size effect of the reinforcement particles on the hardness of the composites is quite significant. The size of the indentation is about twice the size of large particles and 36 times the size of the small particles. The probability of finding a particle under the indenter depends on the volume fraction of the particles, and there is larger variation of the presence of particles at low volume fractions. The hardness of the particle reinforcement plays a role in the measured hardness of the composite. Thus there is a larger variation in the measured hardness at low volume fractions. The interfacial area of the particulate/matrix is higher for the small size composites compared to the large size reinforced composites. The interfacial strength plays a role in the measured hardness of the composites and thus there is a significant size effect of the measured hardness. Large reinforcement composites were found to have higher hardness than the composites with small particles due to better load sharing and less interfacial area.

We also note particularly that the increase in hardness is due to the stiffness of the reinforcement particles. Mullite has an elastic modulus of 143 GPa whereas the elastic modulus of silica is 71 GPa. This difference in modulus is reflected in the observed hardness of the Fe/mullite composites at 20% volume fraction which is similar to the hardness of Fe/silica composites at 30% volume fraction. Also, the increase in hardness with volume fraction of reinforcement is much more significant for the Fe/mullite composites compared to the Fe/silica composites. Since high hardness values indicate better wear resistance from Archard's relation [30], these trends are of interest while examining the wear properties of the composites.

3.5. Wear loss

Fig. 10 shows wear loss as a function of volume fraction and size of the particulates for 25 m/s sliding speed test. In all composites, the wear loss reduced with increasing volume fraction of particulates. We note some significant trends. First, the wear loss of the large particulate reinforcement composites is smaller than the small reinforcement composites. However, the effect of particle size is smaller at higher particle volume fractions. This is in accord with the observation that the hardness of the LM and LO composites is higher than the corresponding SM and SO composites. Next, we observe that the wear loss of the LM composite at 20% volume fraction is *significantly less* than that of the 30% LO composite. This is in spite of the fact that the average hardness of the two composites is the same (92 BHN). Thus the higher stiffness of the mullite reinforcement plays a more significant role than indicated by Archard's equation. Finally, the wear loss of the 15% volume fraction of the SM composite is comparable to that of the 30% volume fraction LO composite even though the hardness of the SM composite at 15% volume fraction is about 35% lower than the hardness of the LO 30% volume fraction composite. This

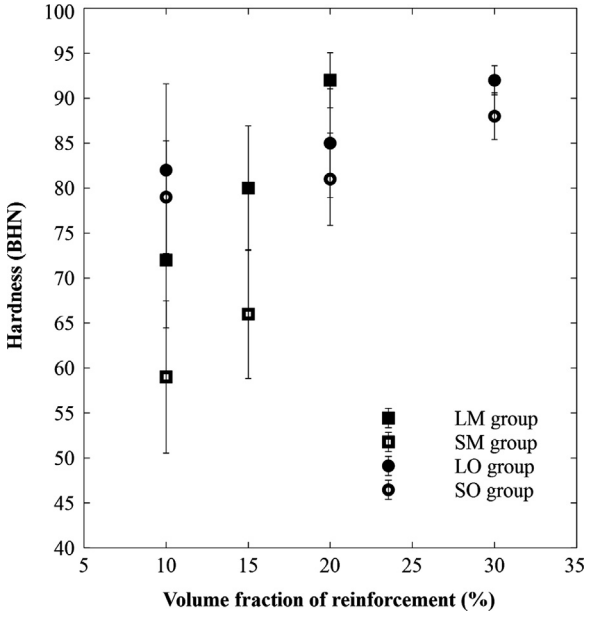

Fig. 9. Hardness of the composites as function of the volume fraction of reinforcements.

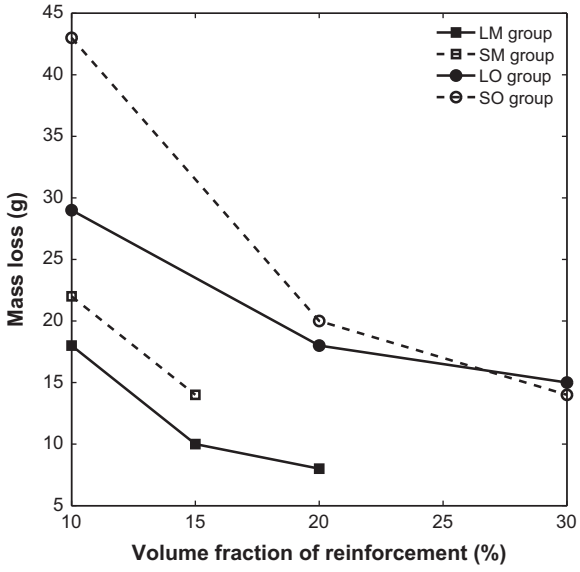

Fig. 10. Wear loss of the composites as a function of volume fraction of the reinforcement at 25 m/s sliding speed.

improvement in wear resistance may be due to several factors in addition to the higher hardness: minimization of load shared by the particulates, reduction of direct metal to metal adhesive contact, earlier formation and stabilization of mechanical mixed tribolayer, work hardening of matrix and increased depth of subsurface deformation [14,20].

The mass loss of the highest volume fraction composites is plotted as a function of the sliding speed in Fig. 11. Even though the wear resistance of the smaller size composites was comparable to that of the large particle composites at lower speeds, it can be seen that they perform markedly worse at higher speeds. The large size silica particulates reinforced composites showed better wear resistance than the small size silica particulates reinforced composites at all volume fractions (10–30%) for all sliding conditions (25–35 m/s). This is possibly due to the deeper embedding of the large size particulate that makes its removal difficult. Our wear results are in good agreement with previous studies, which showed that the bigger particulate size MMCs are better in improving wear resistance by taking more share of contact loads and distributing it to greater depth below contact surface [31,32]. Overall, the Fe/20% mullite (150–250 μm size particulates) composite (LM-C) and the Fe/30% silica (150–250 μm size particulates) composite (LO-C) showed the best wear resistance compared to the other composites at all sliding speeds. The small size particulates are not favorable at higher sliding conditions (30 m/s and 35 m/s) due to their earlier pull out from the matrix. Other mechanisms such as easier breakage of the particulates by dislocation shearing under heavy plastic deformation and subsequent matrix oxidation and removal of the rapidly grown thick oxide film, and sub surface matrix softening by the high frictional temperature conditions may also be operative. The increase of frictional energy dissipated in the form of heat energy at higher sliding speeds softens the matrix and weakens the interface with allowing easier pull out of the particulates. In addition, the rate of oxidation increases causing the growth and removal of an oxide scale resulting in greater wear loss at higher sliding speed conditions [4,33]. This effect is expected to be substantial in small size composites due to the greater interfacial area due to higher number of particulates per unit area.

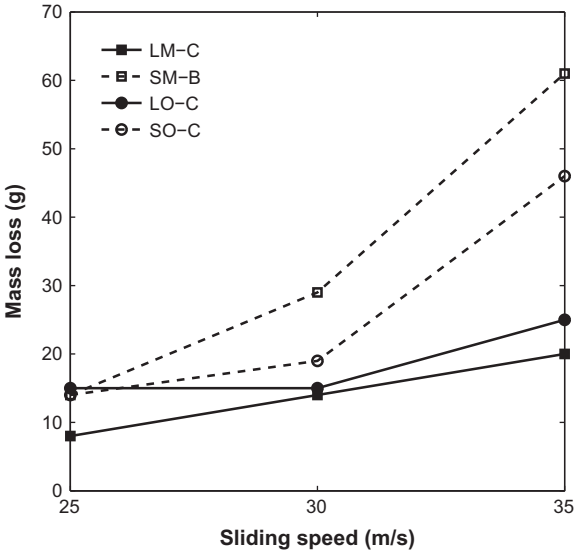

Fig. 11. Wear loss of the highest volume fraction composites as a function of sliding speed.

Thus the properties of the reinforcement are important in the overall wear resistance of the MMC and not just the size and volume fraction of the particulates. However, at higher sliding speeds, the size and volume fraction of particulates are also important.

3.6. Wear patterns

Typical stereo-macrographs of wear tracks of the LO-C composite for the 25 m/s and 35 m/s sliding conditions are shown in Fig. 12. At 25 m/s, grooves running parallel to the direction of sliding were observed on the wear tracks of all the composites which is a typical characteristic of abrasive wear. Particulate pull out, extensive oxide scale, cracks in the matrix and grooves were seen in the macrographs of composites at higher sliding speed conditions (30 m/s and 35 m/s) whereas only grooving is observed at 25 m/s. These wear characteristics confirm that a mixture of wear mechanisms such as delamination, oxidation and abrasive wear are in operation at higher sliding speed conditions (30 m/s and 35 m/s). It is noted that the oxidation and matrix/interface weakening is more severe at higher sliding speeds resulting in higher wear loss as discussed in the previous subsection. The wear mechanism map for steels developed by Lim and Ashby [36] also indicated that oxidation wear is increasingly dominant at higher sliding speed conditions. This effect is more pronounced for small size particulate reinforced composites such as SO-C and SM-B due to the relatively larger interfacial area.

3.7. Braking parameters

In this section we discuss the mean stopping distance and the coefficient of friction of the composites. The other braking parameters of interest: the mean stopping time and the mean torque are directly related to the mean stopping distance and coefficient of friction respectively.

In this section we discuss the influence of volume fraction and size of reinforcements on the mean stopping distance and the coefficient of friction of the composites. The other braking parameters of interest: the mean stopping time and the mean torque

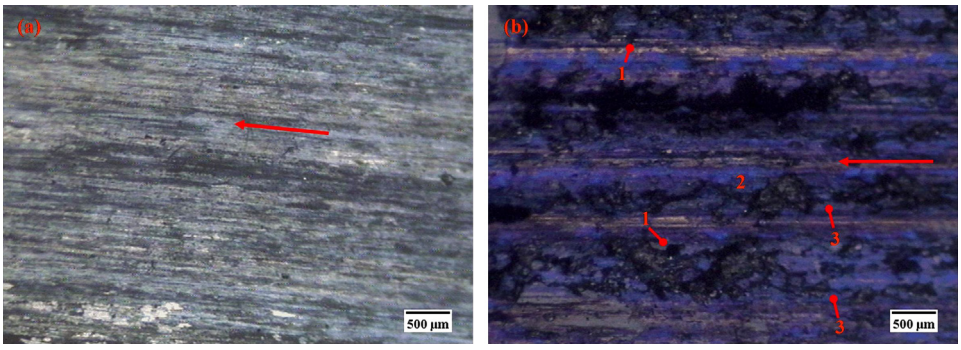

Fig. 12. Macrographs of the LO-C composite: (a) 25 m/s and (b) 35 m/s. The observed features include (1) particulate pull-out (delamination wear), (2) oxidized scale from oxidation wear and (3) matrix cracking. Arrows indicate the direction of sliding.

are directly related to the mean stopping distance and coefficient of friction respectively.

The influence of volume fraction and size of reinforcements on the mean stopping distance for the range of sliding speeds considered is discussed first. The Fe/mullite composite with 15% volume fraction of small sized reinforcement (SM-B) is found to have the smallest stopping distance of all the composites considered in this study (Fig. 13). For comparison, we have also plotted the composites with the best wear resistance from the small particle reinforcement and large particle reinforcement groups for the Fe/silica and Fe/mullite composites. As is to be expected, the mean stopping distance increases with sliding speed due to the higher braking energy. The increase in heat generated at the higher braking energy conditions softens the matrix and weakens the matrix–particle interface. It can be observed that at the lower speeds there is little difference in the stopping distance obtained through the various composites. However, at the highest speed condition, the stopping distance is significantly lower for the Fe/mullite composites compared to the Fe/silica composites. Since the wear loss is also the lowest for these composites, it may be inferred that the higher integrity of the surface allows for greater metal to metal contact and enhances the stopping effectiveness.

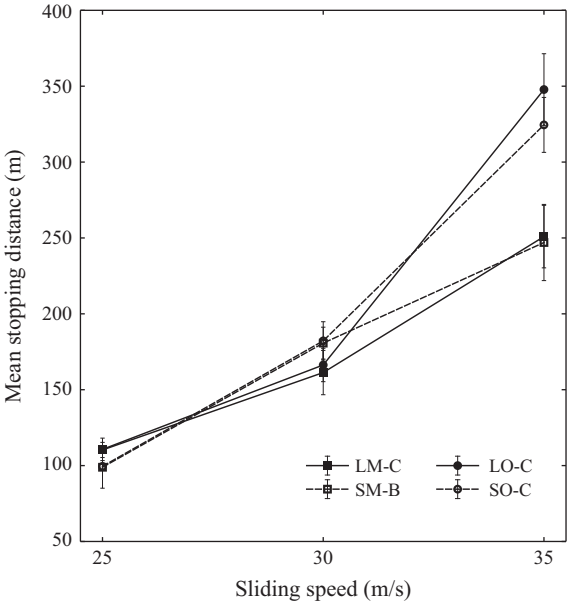

Fig. 13. Mean stopping distance as a function of the sliding speed.

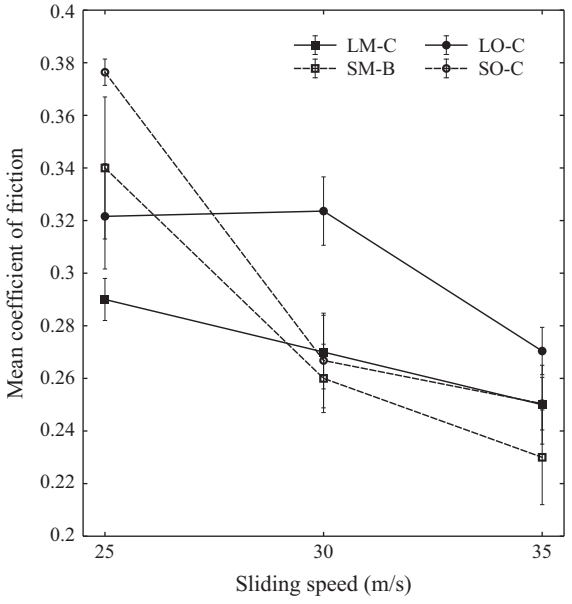

Fig. 14. Mean coefficient of friction as a function of the sliding speed.

The coefficient of friction (COF) for the same set of composites as discussed above is plotted as a function of sliding speeds in Fig. 14. The COF of all the composites decreased as a function of the sliding speed. The decrease in COF with sliding speed is attributed to the increased particulate interface weakening, matrix softening and greater oxidation. Uyyuru et al. [13] also observed a similar behavior in aluminum matrix composite/brakepad tribo-couple. Even though the small reinforcement composites showed significantly higher COF at lower speeds, the decrease with increasing speeds is much more significant than the large reinforcement size composites. In view of this, the large size reinforcement composites should be preferred over the small reinforcement composites.

4. Conclusions

We developed Fe based MMCs using powder metallurgy techniques and studied the tribological properties. We systematically studied the effect of the volume fraction and size of the particulate reinforcement at various high sliding speed conditions. We found that larger particle size reinforcements provided better wear resistance holding all other conditions fixed. Also, higher reinforcement volume fraction of reinforcement provided better wear resistance. The larger size and higher volume fraction composites showed higher hardness which translated to higher wear resistance.

We compared the wear resistance of two reinforcement types. Composites with mullite particles showed smaller wear loss at a lower volume fraction of reinforcement compared to those with silica particles. This is attributed to the greater elastic modulus of the mullite compared to silica which is known to increase the hardness of the composites. However, the wear resistance of the composites with stiffer reinforcements exceeded that explained by increasing hardness. For example, small size Fe/15%mullite composites had comparable wear resistance as large size Fe/30%silica composites at 25 m/s sliding conditions. However, at higher sliding speeds, the larger size reinforcement composites performed much better. An examination of the wear tracks showed that abrasive wear was the main wear mechanism at 25 m/s. A mixed mode of wear with delamination, oxidation and abrasion was observed at higher sliding speed conditions.

When viewed in the context of braking parameters such as mean stopping distance and coefficient of friction, the large reinforcement size composites performed best. Fe/20%mullite composite required the smallest stopping distance of all the composites considered and had a moderately good coefficient of friction which varied little with sliding speed. Other composites such as the small reinforcement sized Fe/mullite and Fe/silica required a short braking distance and had high coefficient of friction at low sliding speeds. However, the braking performance of these composites declined significantly with increasing sliding speed.

Thus, in selecting materials for low wear loss and braking performance, larger size and higher volume fraction reinforcement particles with greater elastic modulus are to be preferred.

Acknowledgments

The authors are grateful to Hindustan Aeronautical Limited, Bangalore for their support in providing access to their testing

facilities for our research work. The authors also thank the anonymous reviewers for their detailed comments.

References

[1] N. Saka, N.K. Szeto, T. Erturk, Friction and wear of fiber reinforced metal-matrix composites, Wear 157 (1992) 339–357.
[2] O.P. Modi, B.K. Prasad, A.H. Yegneswaran, M.L. Vaidya, Dry sliding wear behaviour of squeeze cast aluminium alloy–silicon carbide composites, Mater. Sci. Eng. A 151 (1992) 235–245.
[3] C. Perin, W.M. Rainforth, The effect of alumina fibre reinforcement on the wear of an Al-4.3%Cu alloy, Wear 181–183 (1995) 312–324.
[4] N.B. Dhokey, R.K. Paretkar, Study of wear mechanisms in copper-based SiC_p (20% by volume) reinforced composite, Wear 265 (2008) 117–133.
[5] F.E. Kennedy, A.C. Balbahadur, D.S. Lashmore, The friction and wear of Cu-based silicon carbide particulate metal matrix composites for brake applications, Wear 203–204 (1997) 715–721.
[6] S.G. Sapate, A. Uttarwar, R.C. Rathod, R.K. Paretkar, Analyzing dry sliding wear behaviour of copper matrix composites reinforced with pre-coated SiC_p particles, Mater. Des. 30 (2009) 376–386.
[7] C. Garcia-Cordovilla, J. Narciso, E. Louis, Abrasive wear resistance of aluminum alloy /ceramic particulate composites, Wear 192 (1996) 170–177.
[8] M. Narayan, M.K. Surappa, B.N.P. Bai, Dry sliding wear of Al alloy 2024-Al_2O_3 particle metal matrix composites, Wear 181–183 (1995) 563–570.
[9] H. Akbulut, M. Durmam, F. Yilmaz, Dry wear and friction properties of δ-Al_2O_3 short fiber reinforced Al-Si (LM 13) alloy metal matrix composites, Wear 215 (1998) 170–179.
[10] L. Ceschini, G.S. Daehn, G.L. Garagnani, C. Martini, Friction and wear behavior of C^4 Al_2O_3/Alcomposites under dry sliding conditions, Wear 216 (1998) 229–238.
[11] H. Ahlatci, T. Kocer, E. Candan, H. Cimenoglu, Wear behaviour of Al/($Al_2O_3p+SiC_p$) hybrid composites, Tribol. Int. 39 (2006) 213–220.
[12] L.J. Yang, Wear coefficient equation for aluminium-based matrix composites against steel disc, Wear 255 (2003) 579–592.
[13] R.K. Uyyuru, M.K. Surappa, S. Brusethaug, Effect of reinforcement volume fraction and size distribution on the tribological behavior of Al-composite/brake pad tribo-couple, Wear 260 (2006) 1248–1255.
[14] R.L. Deuis, C. Subramanian, J.M. Yellup, Dry sliding wear of aluminum composites—a review, Compos. Sci. Technol. 57 (1997) 415–435.
[15] A. Kelly, Composite materials after seventy years, J. Mater. Sci. 41 (2006) 905–912.
[16] C.S. Ramesha, C.K. Srinivas, B.H. Channabasappa, Abrasive wear behaviour of laser sintered iron-SiC composites, Wear 267 (2009) 1777–1783.
[17] M. Chandrasekaran, U.P. Singh, Sintered iron-based antifriction materials with added β-SiC, Wear 206 (1997) 1–7.
[18] T. Ram Prabhu, V.K. Varma, S. Vedantam, Effect of SiC volume fraction and size on dry sliding wear of Fe/SiC composites for high sliding speed applications, Wear 309 (2014) 1–10.
[19] K.M. Shorowordi, T. Laoui, A.S.M.A. Haseeb, J.P. Celis, L. Froyen, Microstructure and interface characteristics of B_4C SiC, and Al_2O_3 reinforced Al matrix composites: a comparative study, J. Mater. Proc. Technol. 142 (2003) 738–743.
[20] J. Li, B.Y. Zong, Y.M. Wang, W.B. Zhuang, Experiment and modeling of mechanical properties on iron matrix composites reinforced by different types of ceramic particles, Mater. Sci. Eng. A 527 (2010) 7545–7551.
[21] E. Pagounis, M. Talvitie, V.K. Lindroos, Influence of matrix structure on the abrasion wear resistance and toughness of a hot isostatic pressed white iron matrix composite, Met. Mater. Trans. A 27 (1996) 4183–4191.
[22] P.K. Rohatgi, B.F. Schultz, A. Daoud, W.W. Zhang, Tribological performance of A206 aluminum alloy containing silica sand particles, Tribol. Int. 43 (2010) 455–466.
[23] J. Hemanth, Quartz (SiO_2p)reinforced chilled metal matrix composite (CMMC) for automotive applications, Mater. Des. 30 (2009) 323–329.
[24] J. Hemanth, Abrasive and slurry wear behavior of chilled aluminum alloy (A356) reinforced with fused silica (SiO_2p) metal matrix composites, Compos. Part B 42 (2011) 1826–1833.
[25] I.A. Ibrahim, F.A. Mohamed, E.J. Lavernia, Particulate reinforced metal matrix composites—a review, J. Mater. Sci. 26 (1991) 1137–1156.
[26] P.J. Blau, H.M. Meyer, Characteristics of wear particles produced during friction tests of conventional and unconventional disc brake materials, Wear 255 (2003) 1261–1269.
[27] M. Asif, K. Chandra, P.S. Misra, Development of iron based Brake friction material by hot powder preform forging technique used for medium to heavy duty applications, J. Miner. Mater. Char. Eng. 10 (2011) 231–244.
[28] A. Daoud, M.T.A. El-khair, Wear and friction behavior of sand cast brake rotor made of A359 - 20 vol% SiC particle composites sliding against automobile friction material, Tribol. Int. 43 (2010) 544–553.
[29] P.H.S. Tsang, M.G. Jacko, S.K. Rhee, Comparison of chase and inertial brake dynamometer testing of automotive friction materials, Wear 103 (1985) 217–232.
[30] J.F. Archard, Contact and rubbing of flat surfaces, J. Appl. Phys. 24 (1953) 981.
[31] F.M. Hosking, F.F. Portillo, R. Wunderlin, R. Mehrabian, Composites of aluminum alloys: fabrication and wear behavior, J. Mater. Sci. 17 (1982) 477–498.
[32] S. Chung, B.H. Hwang, A microstructural study of the wear behaviour of SiC_p/Al composites, Tribol. Int. 27 (1994) 307–314.
[33] S. Kumar, V. Balasubramanian, Developing a mathematical model to evaluate wear rate of AA7075/SiC_p powder metallurgy composites, Wear 264 (2008) 1026–1034.
[36] S.C. Lim, M.F. Ashby, Overview no. 55 wear-mechanism maps, Acta Metall. 35 (1987) 1–24.